



Effect of transverse magnetic field on arc characteristics and droplet transfer during laser-MIG hybrid welding of Ti-6Al-4 V

Chen Yue¹ · Annan Yin¹ · Dehua Huang¹

Received: 12 March 2021 / Accepted: 18 September 2021 / Published online: 30 September 2021
© The Author(s), under exclusive licence to Springer-Verlag London Ltd., part of Springer Nature 2021

Abstract

In this study, the effect of the transverse magnetic field on the arc characteristics and droplet transfer behavior is investigated during Laser-MIG hybrid welding of Ti-6Al-4 V. Especially, transverse magnetic fields with 0 mT, 8 mT, 16 mT, 24 mT, and 32 mT are studied. Results indicate that an appropriate magnetic field can increase the stability of arc characteristics, improve the droplet detachment efficiency, and reduce the welding defects such as incomplete fusion and undercut. By applying 24-mT transverse magnetic field, the maximum arc area can decrease by 48.7% with its variance changing from 2.81 to 1.06 mm², indicating that an appropriate transverse magnetic field can shrink the arc and improve its stability. The reason of arc shrinkage is that the electric streamline in the arc rotates away from the laser side to the droplet side due to the influence of external magnetic field. On the other hand, the droplet transfer process becomes more uniform under the appropriate magnetic field. This phenomenon is mainly attributed to the change of Lorentz force direction during droplet rotation, which resultantly increases effective detachment energy. This phenomenon leads to the reduction of the contact time between droplet and molten pool. The droplet transfer form changes from short-circuit transfer to meso-spray transfer under 24-mT magnetic field because of the reduction of the contact time. Therefore, the incomplete fusion and undercut disappears. At last, the appropriated magnetic field parameters during the laser-MIG parameters (2 kW, 160 A, 2 m/min) are concluded as $B = 24$ mT.

Keywords Transverse magnetic field, · Laser-MIG hybrid welding, · Ti-6Al-4 V, · Droplet transfer, · Arc characteristics

1 Introduction

Titanium alloys have been used in aerospace, electronic communication, precision instruments, and petrochemical industries owing to their low density, high-specific strength, good ductility, and excellent mechanical properties at high temperatures [1, 2]. The hybrid laser-arc welding technique has been widely recognized because it combines both laser and arc welding, and exhibits good joint

bridging performance, deep weldability, and high welding efficiency [3] {Gao, 2016 #5; Zhengwu, 2020 #66}. In recent years, this technique used to weld Ti-6Al-4 V, which is one of the most widely used titanium alloys owing to its stable structure and good connection performance [4–6].

However, several problems arise during the laser-MIG hybrid welding of Ti-6Al-4 V, such as the formation of weld bead, welding stability, and weld defects [7]. Recent studies on these concerns indicate that the stability of the welding process and the appearance of welding beads are influenced by the arc performance [8] and droplet transfer behavior [9]. Liu et al. [10] demonstrated that the distance between the laser and arc (DLA) could affect the plasma behavior and transfer mode and hence of the hybrid welding; the welding penetration depth is changed. Zhang et al. [11] observed the plasma characteristics and droplet transfer in a CO₂ laser-GMAW-P hybrid welding and concluded that the droplet size and formation time increased with changes in the electromagnetic force, resulting in an off-axis droplet phenomenon. Wang et al. [12] demonstrated that a curved channel

✉ Chen Yue
yue30008@126.com

Annan Yin
annan_yin@hust.edu.cn

Dehua Huang
huangdehua@hust.edu.cn

¹ The State Key Laboratory of Digital Manufacturing Equipment and Technology, School of Mechanical Science and Engineering, Huazhong University of Science & Technology, Wuhan 430074, People's Republic of China

forms between the welding wire and keyhole during the fiber laser-MIG hybrid welding of ZL114. Chen et al. [13] investigated the influence of the welding position in CO₂ laser-arc hybrid welding and concluded that the mean droplet transfer frequencies affected the appearance of the welding bead. Tang et al. [14] indicated that the plasma temperature increased with an increase in the amount of shielding gas, thereby increasing the penetration depth and weld width in laser-MIG hybrid welding. Based on the above studies, it can be concluded that the arc performance and metal transfer behavior significantly affect the microstructure properties of the weld, welding penetration depth, and welding bead appearance.

Therefore, the arc performance and droplet transfer behavior must be managed to control the weld bead quality. A magnetic field has been used to control the arc performance and droplet behavior to regulate and manage the welding process [15, 16] {Chen, 2020 #82; Zhengwu, 2020 #66; Sun, 2018 #86}. However, in laser welding, the welding process is affected when the magnetic field threshold exceeds 200 mT. Chen et al. [17] investigated the influence of a 240-mT magnetic field on the laser welding of dissimilar materials and reported that the magnetic field was beneficial in the weld bead appearance and microstructure. Avilov et al. [18] observed the appearance of welding beads under alternating magnetic fields during laser beam welding and concluded that the alternating magnetic field had a beneficial effect on the inhibiting gravitational drop-out and sagging of the weld. However, the welding process was considerably affected when the magnetic field threshold was below 50 mT for arc welding. Guan et al. [19] demonstrated that the external magnetic field (12.5sternal frequency significantly impacted the arc shape and movement, which affected the arc temperature gradient and undercooling degree, thereby affecting the weld appearance and mechanical properties in GMAW welding. Chang et al. [20] indicated that a synchronous electromagnetic field, including low-frequency magnetic fields for the arc-burning phase and high-frequency magnetic fields for the short-circuit phase, can be introduced to the short-circuit GMAW to improve the frequency of metal transfer and reduce spatter. Sun et al. [21] reported that magnetic arc oscillations could alter the arc voltage and cause the weld current to flow through the sidewalls, thereby increasing sidewall penetration and redistribution of arc heat. Wang et al. [22] demonstrated that while the arc pressure at the bottom of the molten pool decreased, that of the sidewall improved the morphology through TIG welding

via a transverse magnetic field (4 mT). The voltage of the magnetic arc is invariably high compared to a non-magnetic arc, which decreases with an increase in the welding current. Moreover, laser-MIG hybrid welding is profoundly influenced by the external magnetic field with a threshold below 50 mT. Zhang et al. [23] demonstrated that, in the laser-MIG hybrid welding of 316 L, an external longitudinal magnetic field (16 mT) increases the stability of the welding arc and affects the force on the droplet transfer. Zhu et al. [24] further indicated that a laser and magnetic field (16 mT) combined induced a periodically altered axial asymmetry of the arc along the welding direction in the laser-MIG hybrid welding of 316 L. Based on the literature above, we can conclude that an appropriate magnetic field significantly impacts the arc performance and droplet behavior in laser-MIG hybrid welding.

However, there are only a few systematic studies on the arc performance and metal transfer in transverse magnetic field-assisted laser-MIG hybrid welding of Ti-6Al-4 V. In this study, we demonstrate the influence of an external magnetic field on the arc performance and droplet transfer in laser-MIG hybrid welding for Ti-6Al-4 V, which can be used to improve welding stability and weld quality.

2 Experimental procedures

2.1 Materials

A 4-mm-thick Ti-6Al-4 V titanium alloy base metal and a 1-mm-thick Ti-6Al-4 V filler wire were used in this study. The chemical compositions of the base metal and wire are listed in Table 1. The oil contamination on the surface of the sheets was removed using acetone, before welding. Surface treatment was carried out to remove the oxidation film and residual acetone by laser cleaning using a 300-W laser device. To protect the welding joint from oxidation, pure argon was used as the shielding atmosphere, with a flow rate of 2 m³/h.

2.2 Welding preparation

A 4-kW fiber laser (IPG RYL-4000), capable of providing a continuous wave output with a 1.07- μ m laser emission wavelength, was used to weld the Ti-6Al-4 V plates by bead welding. The laser spot, with a 0.3-mm diameter, was focused at the center of the sheet. A Fronius TPS

Table 1 Chemical composition of the base metal and the wire (wt. %) [6]

Element	Al	V	N	H	O	Fe	C	Ti
Base metal	5.5–6.8	3.5–4.5	0.05	0.015	0.20	0.30	0.10	Bal
Weld wire	5.8	4.2	0.05	0.015	0.20	0.30	0.10	Bal

4000 digital power controller was used as the MIG welding power controller. A transverse external magnetic field was generated using permanent magnet blocks, which can provide a maximum magnetic field of 60 mT. To ensure the external magnetic field is stable during the high-speed camera (HSC) shoot, the sheets were placed between two magnet blocks, as shown in Fig. 1. Because the magnetic blocks and laser head were kept stationary during welding, the distribution of the magnetic induction lines was perpendicular to the welding direction. The magnetic field intensity was adjusted by changing the distance between the magnetic block and weld plate. During the welding process, the control variable method was used to study the effect of the magnetic field on the droplet transfer and arc performance. The main welding parameters used during hybrid welding are listed in Table 2. To observe the droplet and arc, the HSC was placed perpendicular to the welding direction, and the lens parallel to the welding joint.

Table 2 Main welding parameters during the hybrid welding

Laser power (kW)	Welding current (A)	Welding speed (m/min)	Protection gas flow (m ³ /h)	DLA (mm)	Magnetic intensity (mT)
2	160	2	2	3	0–32

2.3 Image processing

The images obtained from the HSC were processed through segmentation to reduce the influence of the laser plasma and molten pool. Additionally, graying and media filtering were used to eliminate the influence of the surrounding laser plasma and other noises. Furthermore, binarization was used to obtain the area of the arc. Finally, the statistical result of the pixel number was used to output the area of the arc. The frequency of the HSC was 5000 Hz, where each image stands for 0.2 ms, as shown in Fig. 2.

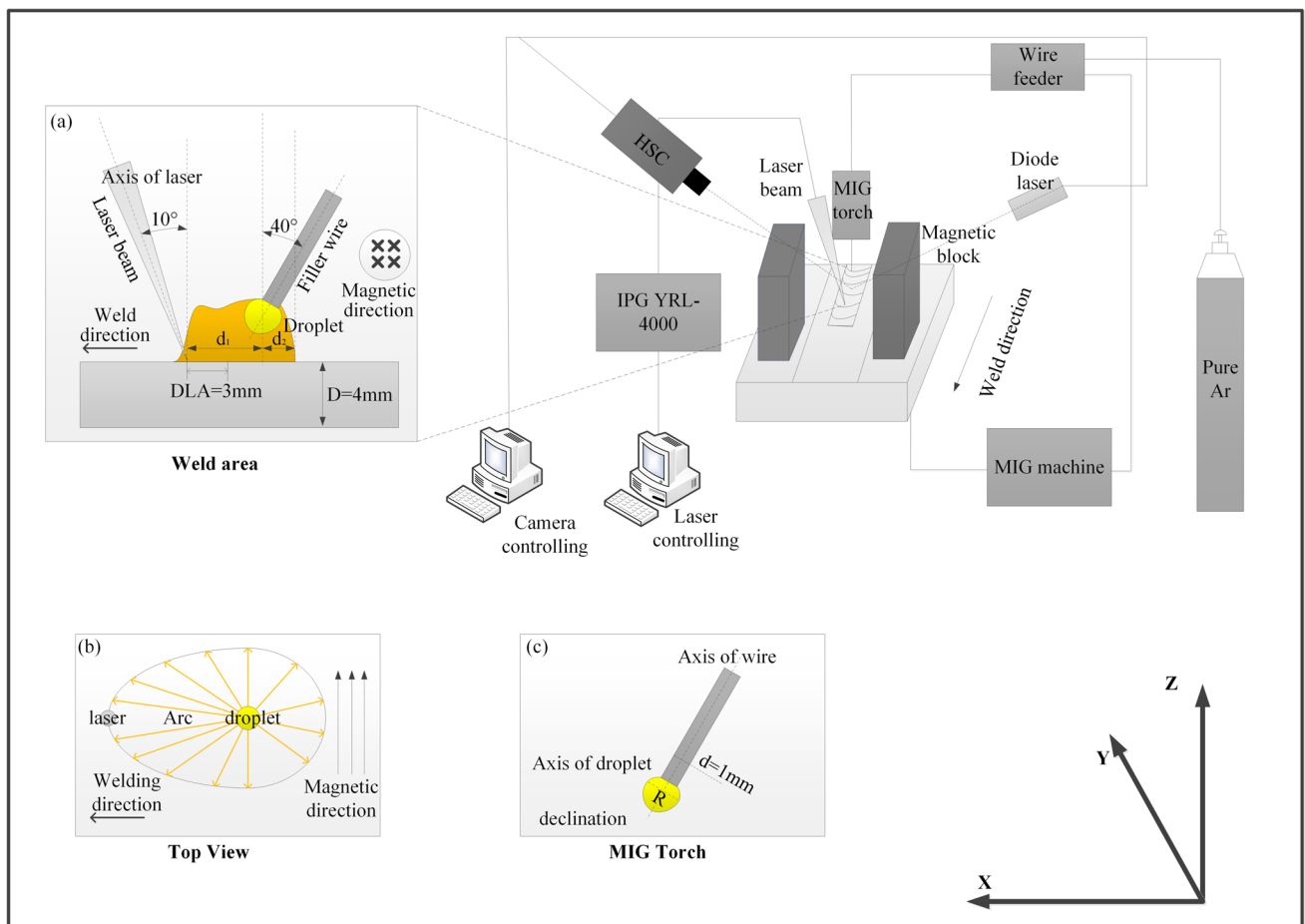


Fig. 1 Schematic of the magnetic field assisted laser-MIG hybrid welding. **a** The magnetic field assisted laser-MIG welding system. **b** The top view of the weld structure. **c** The weld torch structure

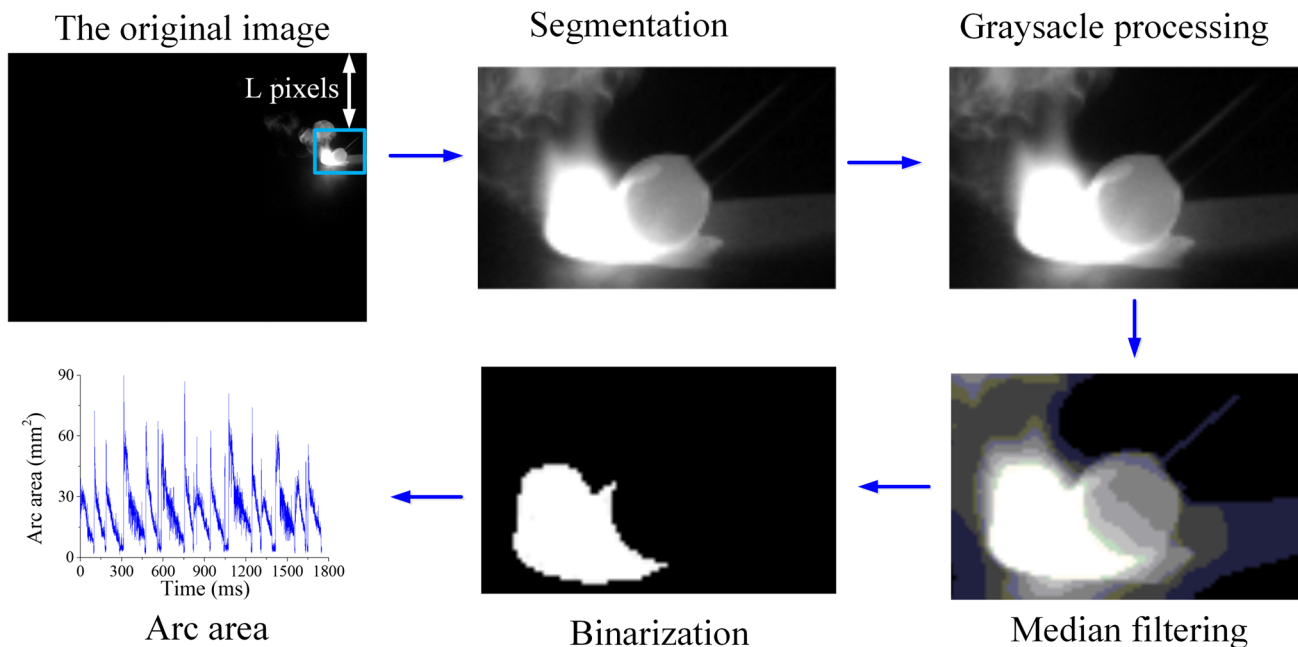


Fig. 2 The arc features extraction processing

The number of pixels within 1 mm² was used as the output to calculate the total arc area. Additionally, median filter, peak seeking, elimination of accompanying peaks, and curve fitting were used to obtain the mean maximum area and variance of the arc area under varying magnetic fields.

3 Theoretical background

In laser-MIG hybrid welding, the weld cross-section performance is mainly influenced by the heat resource, weld pool flow, and droplet transfer. The heat input (Q) is mixed

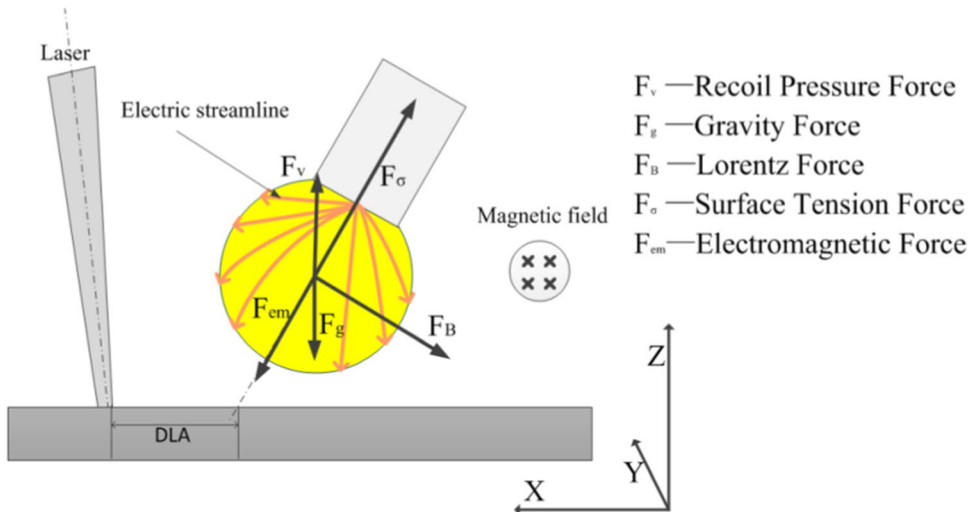
by the laser heat (Q_{laser}) and arc heat (Q_{arc}) inputs, and is given as follows:

$$Q = Q_{laser} + Q_{arc} = \frac{\eta_1 P_{laser} + \eta_2 UI}{v} \tag{1}$$

where P is the laser power, U is the arc voltage, I is the welding current, η_1 and η_2 are the efficiencies of the laser beam and arc power, respectively, and v is the welding speed.

Multiple forces such as surface tension, gravity, plasma flow force, electromagnetic force, and external magnetic force act on the droplet during hybrid welding, as shown in Fig. 3.

Fig. 3 Forces acting on the droplet in the transverse magnetic field-assisted Laser-MIG hybrid welding



As the welding wire melts, a surface tension force is formed between the molten metal and plasma, which is given as follows:

$$F_{\sigma} = 2\pi r_w \sigma \tag{2}$$

where r_w is the wire radius and σ is the surface tension coefficient.

The gravity is given as follows:

$$F_g = \frac{4}{3}\pi r^3 \rho g \tag{3}$$

where r is the droplet radius, ρ is the droplet density, and g is the acceleration due to gravity.

The metal vapor formed during the welding process generates a force, which is given as follows:

$$F_v = \left\{ \begin{array}{l} \frac{1}{4\pi R_h^2} C_D A p \frac{2}{m} V^2 \left(\frac{N_a K_B T_s^{3/2}}{M_a B_o} \right) \exp(-U/T_s) \exp(-D^2/2R_h^2) (D \leq R_h) \\ o(D \geq R_h) \end{array} \right\} \tag{4}$$

where R_h is the distribution parameter of the metal vapor, V_0 is a constant, N_a is Avogadro’s constant, K_B is the Boltzmann constant, T_s is the surface temperature of the molten zone, M_a is the molecular weight, U is a calculated constant, and D is the distance between the laser and the arc.

The electromagnetic force is one of the most important forces acting on the droplet during hybrid welding, which is produced by the current passing through the droplet and welding arc, and is given as follows:

$$F_{em} = \frac{\mu_0 I^2}{4\pi} \left[\ln \frac{r \sin \theta}{r_w} - \frac{1}{4} - \frac{1}{1 - \cos \theta} + \frac{2}{(1 - \cos \theta)^2} \ln \frac{2}{1 + \cos \theta} \right] \tag{5}$$

where I is the welding current, μ_0 is the permeability of free space, r and r_w are the radii of the droplet and the wire, respectively, and θ is the angle of the arc-cover area.

The additional magnetic force, produced by the external Lorentz force, that is, the external magnetic field acting on the current passed through the droplet and the welding arc, is another one of the important forces formed when the magnetic field acts on the hybrid welding process and is given as follows:

$$F_B = \frac{\int_0^L B I dl}{r} = \frac{\pi B I r}{2} \tag{6}$$

where B is the extra magnetic field magnitude, I is the welding current, L is the length of the arc influence area, and r is the radius of the droplet.

4 Result and discussion

4.1 Effects of the external magnetic field on the weld appearance

The effect of different external magnetic fields on the weld appearance is listed in Table 3. The appearance of the weld without an external magnetic field under high-speed welding (2 m/min) was not uniform and straight, and showed incomplete fusion regions and undercuts, as indicated in the images, which may be caused by insufficient droplet transfer frequency. The weld quality between a magnetic frequency threshold of 8–24 mT indicated an appropriate external magnetic field with a positive influence on the weld appearance. The figures show that the incomplete fusion gradually disappears, and the weld becomes straight and uniform as the magnetic field intensity increases, indicating that the weld quality improves under an appropriate external magnetic field. Welding defects such as spatter reappear, and the weld profile was not uniform under an excessive external magnetic field, indicating that an excessive external magnetic field negatively impacts the weld quality.


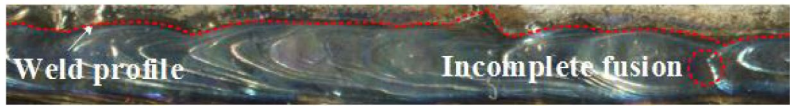
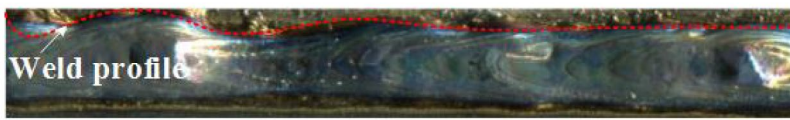
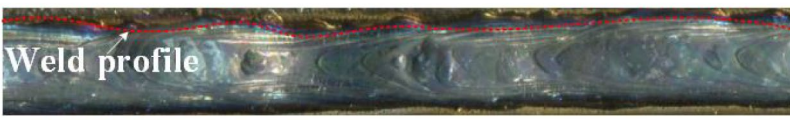
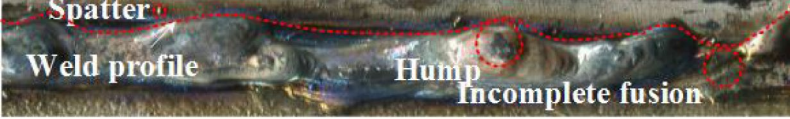
4.2 Effects of the external magnetic field on the arc characteristics

4.2.1 Effects of the external magnetic field on the stable arc performance

The effects of different external magnetic fields on the performance of a stable arc are shown in Fig. 4. During hybrid welding, the laser attracts and stabilizes the arc. d ($d = d_1 + d_2$) is the arc length, representing arc shrinkage, where d_1 and d_2 are the forward and backward arc lengths, respectively. The external magnetic field benefits arc shrinkage only when $d_1 > d_2$, else the magnetic field causes arc divergence and instability, indicating that d , d_1 , and d_2 are inconstant values under different magnetic fields. Therefore, the average value of d must be calculated to identify the arc performance during hybrid welding.

As seen in Fig. 4a, the arc is always oriented toward the laser direction without an external magnetic field. d changes by 8.35%, from 8.1 to 8.8 mm, in four adjacent cycles, indicating an unstable arc during hybrid welding. Meanwhile, when $d_1 = 6.8$ mm, $d_2 = 1.7$ mm, and $d_1 > d_2$, the arc is in the forward situation owing to the laser attraction. Figure 4b and c show that the external magnetic fields of 8–16 mT can stabilize the arc. d decreases from 5.3 to 4.3 mm as the magnetic field increases, where $d_1 = 3.2$ mm, $d_2 = 1.6$ mm, and $d_1 > d_2$, indicating that the

Table 3 The weld appearance under different external magnetic field

External magnetic field	Weld appearance
0 mT	 Weld profile, Incomplete Fusion, Undercut, 3 mm scale bar
8 mT	 Weld profile, Incomplete fusion
16 mT	 Weld profile
24 mT	 Weld profile
32 mT	 Spatter, Weld profile, Hump, Incomplete fusion

arc spreads perpendicular to the welding direction rather than the laser direction, which shrinks and condenses at the end of the welding wire as the magnetic field increases. At 24 mT (Fig. 4d), d is 2.7 mm and $d_1 = d_2 = 1.4$ mm, indicating that the arc is compressed to its maximum, which causes energy aggregation, increases the unit energy density and energy utilization efficiency, and leads to a uniform weld and increase in penetration. Furthermore, the shape of the arc changes from a bell to a dish with a very short arc length, indicating that the droplet transfer form changes from short-circuit transfer to meso-spray transfer. As seen in Fig. 4e, with an external magnetic field of 32 mT, d is 4.1 mm and larger than that under 24 mT, where $d_1 = 1.6$ mm, $d_2 = 2.5$ mm, and $d_1 < d_2$, indicating that the arc diffuses. The arc deflection was observed to be more serious in this set of experimental parameters.

In conclusion, the arc is unstable during high-speed hybrid welding, and an appropriate external magnetic field (24 mT) can effectively improve the stability and condense the arc. Conversely, an excessive external magnetic field (32 mT) causes arc divergence, resulting in a serious arc deflection.

4.2.2 Influence of the external magnetic field on the arc characteristics

In a gas medium, an arc is a strong and lasting discharge phenomenon between two electrodes, or between electrodes

and the base metal at a certain voltage. The physical nature of the arc is charged particles along with the current and is regarded as the aggregation of the electric streamline, which can be significantly affected by an external magnetic field. The external Lorentz force F_B and electromagnetic force F_{em} are the most important forces during hybrid welding.

In laser-MIG hybrid welding, the electromagnetic force F_{em} from the laser to the droplet is the main force acting on the arc electric streamline. The arc is attracted by the laser in the forward welding direction. The arc length was close to the DLA, as shown in Fig. 5a. When an appropriate magnetic field is introduced, the external Lorentz force, F_B affects the arc, which according to the left-hand rule, is perpendicular to the electric streamline. The external Lorentz force is backward and downward on the forward electric streamline, and backward and upward on the backward electric streamline. This phenomenon causes the electric streamline in the arc to rotate away from the laser direction, and the arc shrinks and gathers under the welding wire when the resultant force of the external Lorentz force is backward and downward, especially under the external magnetic field of 24 mT. This improves the stability of the arc and energy efficiency, as shown in Fig. 5b. However, as the external magnetic field increases, the arc gradually moves against the welding direction. Furthermore, when an excessive magnetic field (32 mT) is added, the direction of the resultant external Lorentz force for the arc is backward and upward. The heat

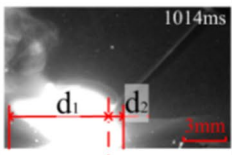
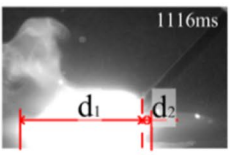
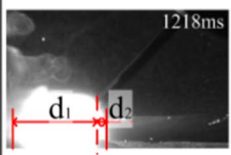
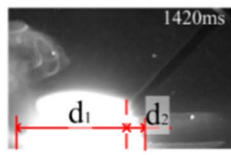
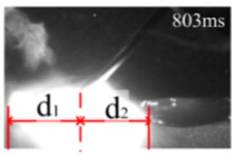
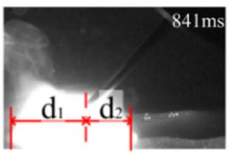
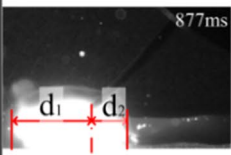
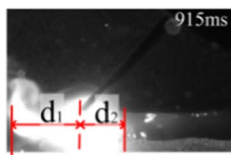
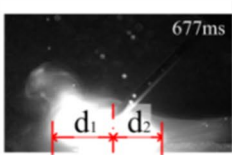
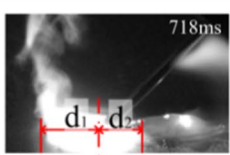
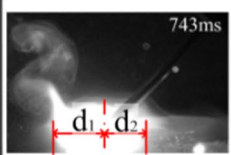
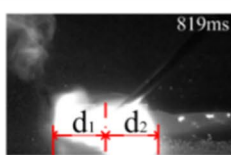
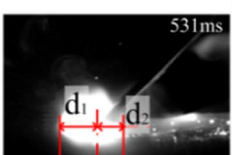
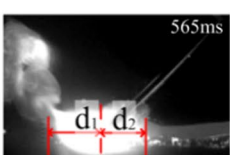
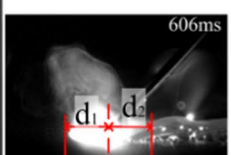
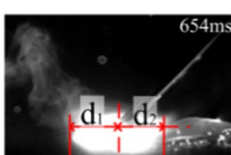
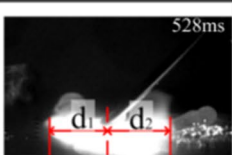
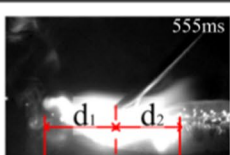
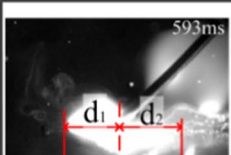
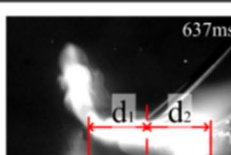
Magnetic Field	Arc Performance				Current Distribution
(a) 0 mT					$d_1 > d_2$
(b) 8 mT					$d_1 > d_2$
(c) 16 mT					$d_1 > d_2$
(d) 24 mT					$d_1 = d_2$
(e) 32 mT					$d_1 < d_2$

Fig. 4 Effects of external magnetic field on the performance of the arc

on the wire increases considering the arc gathers and climbs along at the end of the wire when the F_B is upward, causing the arc to separate into two parts. Finally, the arc became unstable. The influence of an excessive magnetic field on the arc performance is shown in Fig. 5c.

4.2.3 Effects of magnetic field on the maximum of stable arc and arc stability

Image processing was used to analyze changes in the arc area with time under different external magnetic fields, as seen in Fig. 6. The relationship between the arc area and time, without an external magnetic field, is shown in Fig. 6a. The cycle of changes in the arc area change consists of unstable values, and the maximum area of the static arc showed an obvious gradient change. The average and maximum arc change cycles were 88.31 ms and 89.83 mm², respectively, which indicates a long arc change cycle and arc diffusion.

At the end of each cycle, the arc disappears for a long time, representing long arc extinguishing time and instability. As seen in Fig. 6b, at 8 mT, the cycle of the arc area change was 61.91 ms and the maximum area was 58.87 mm², which indicates that the amplitude becomes smaller and the cycle becomes shorter compared to that under 0 mT. However, long arc extinguishing time exists during welding under an external magnetic field of 8 mT, during which the amplitude decreases and the long arc extinguishing time disappears when the amplitude reaches 16 mT and 24 mT, as shown in Figs. 6c and d. The cycle of arc area varied slightly from 46.33 to 44.61 ms, indicating that the change of arc area became more uniform during the process. As seen in Fig. 6e, at 32 mT, the long arc extinguishing time reappears in each cycle, and the area of arc mutates. The maximum area of the arc was 175.81 mm², which is much larger than that under 0 mT. Moreover, the stability of the arc weakens under these

	(a) Without Magnetic field	(b) Appropriate Magnetic field	(c) Excessive Magnetic field
Electric streamline			
Direction of current	$d_1 > d_2$	$d_1 = d_2$	$d_1 < d_2$
Distribution of electric streamline	Attracted by laser Towards Laser	Under wire Towards base metal	Under wire Towards wire

Fig. 5 The external Lorentz force on the arc under a different magnetic field, the arc performance changed with the different magnetic field with the Lorentz force

parameters. Furthermore, the surface quality of the welding beam was also affected.

The varying arc area average peak value represents the stability of the arc, whereas the average peak value represents the property of arc shrinkage. As seen in Fig. 7, the average peak value of arc size decreases by 58.5%, from 37.33 to 15.49 mm², as the magnetic field increases from 0 to 16 mT, and increases by 54.8%, from 15.49 to 23.99 mm², as the magnetic field increases from 16 to 32 mT. This indicates that the arc shrinks as the magnetic field increases, and diffuses under the excessive magnetic field. The variance in the arc area average peak value decreases by 62.3% from, 2.81 to 1.06 mm², as the magnetic field increases from 0 to 24 mT, and increases by 74.5%, from 1.06 to 1.85 mm², as the magnetic field increases from 24 to 32 mT. This indicates that arc stability improves with an appropriate magnetic field (8–24 mT) and decreases under the excessive magnetic field (32 mT).

In conclusion, as the appropriate external magnetic field (0–24 mT) increases, the cycle of the arc area change becomes shorter, the amplitude becomes smaller, and the change in the arc area tends to become more uniform. Furthermore, the maximum area of the arc is smaller than that without an external magnetic field, indicating that the arc shrinks under the action of an external magnetic field. Conversely, the arc stability worsens under an excessive external magnetic field (32 mT), and the maximum area of the stable arc becomes larger.

4.3 Effects of external magnetic field on the droplet transfer behavior

4.3.1 Effects of external magnetic field on the droplet transfer performance

The process of droplet transfer, which is a short-circuit transfer, is shown in Fig. 8. The droplet is first directed toward the laser. As the droplet grew, the direction was kept consistent with that of the welding wire, with time. The droplet slowly grew on the welding wire and separated from the wire when it came in contact with the molten pool, considering the wire was in direct contact with the molten pool. This transfer produces a spatter and a hump.

Figure 9 shows the droplet transfer performance under different external magnetic fields. The droplet behavior under high-speed hybrid welding without an external magnetic field is shown in Fig. 9a. The diameter of the droplet was 1.835 mm, indicating a large droplet detachment size. As seen in Fig. 9b, an external magnetic field of 8 mT was not sufficient to change the droplet transform, and the droplet moved toward the weld plate. Herein, the droplet detachment diameter was 1.578 mm, which is larger than the wire diameter. The droplet transfer performance at 16 mT was similar to that at 8 mT, as seen in Fig. 9c. As the amplitude of the external magnetic field reached 24 mT, the external magnetic field effectively improved the droplet transfer efficiency, as seen in Fig. 9d. The droplet was inclined

Fig. 6 Effects of external magnetic field on the change of the arc area

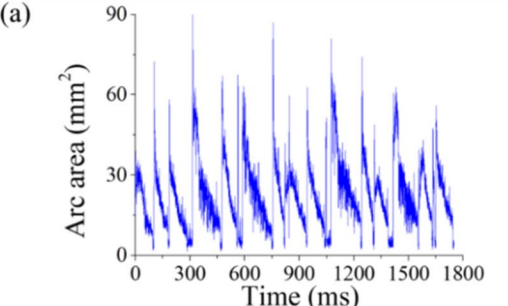
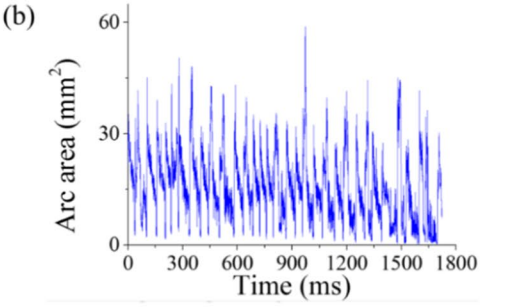
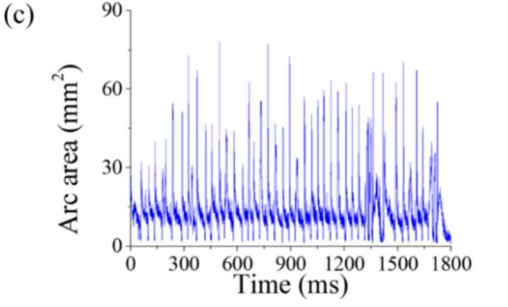
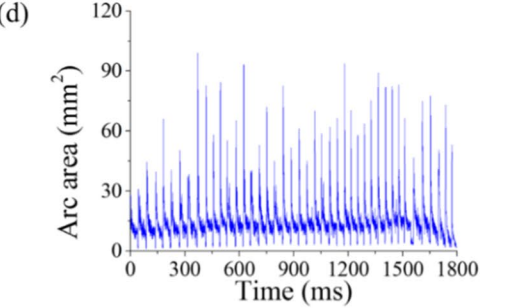
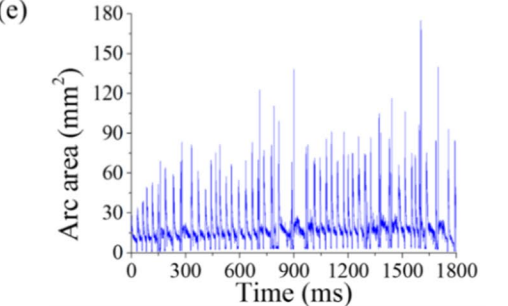
Magnetic field	Arc area vs time diagram	Arc change period
0 mT	(a) 	88.31 ms
8 mT	(b) 	61.19 ms
16 mT	(c) 	46.33 ms
24 mT	(d) 	44.61 ms
32 mT	(e) 	27.38 ms

Fig. 7 The maximum area and the variance of arc area under different external magnetic fields

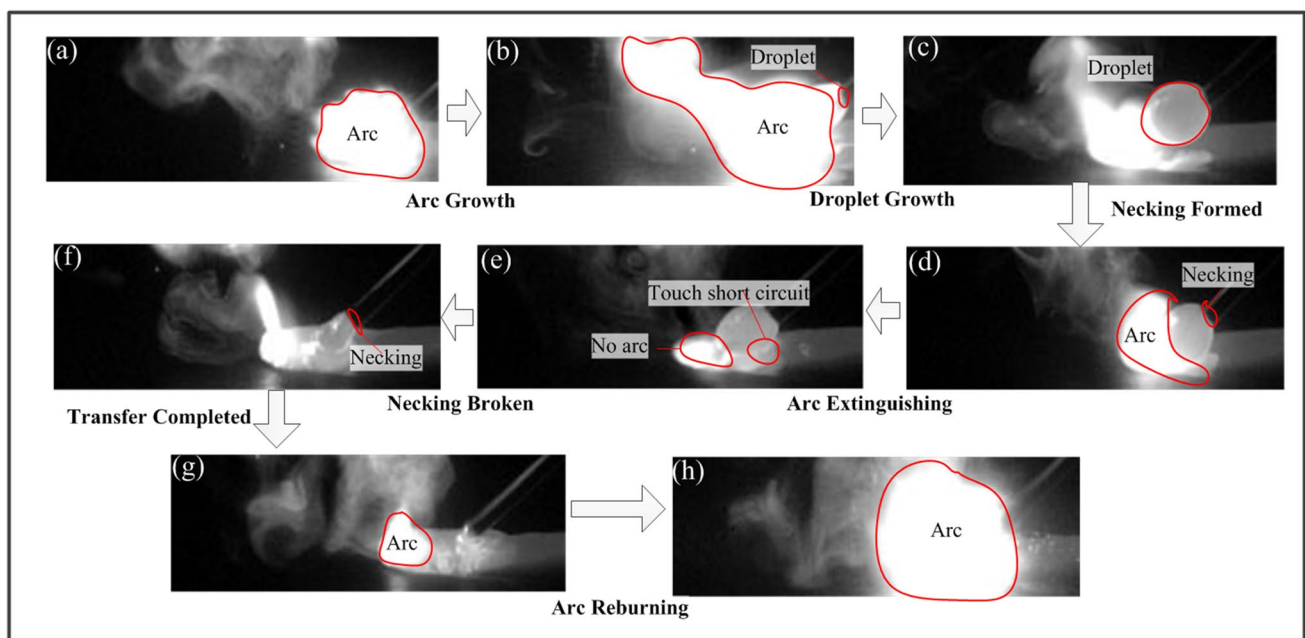
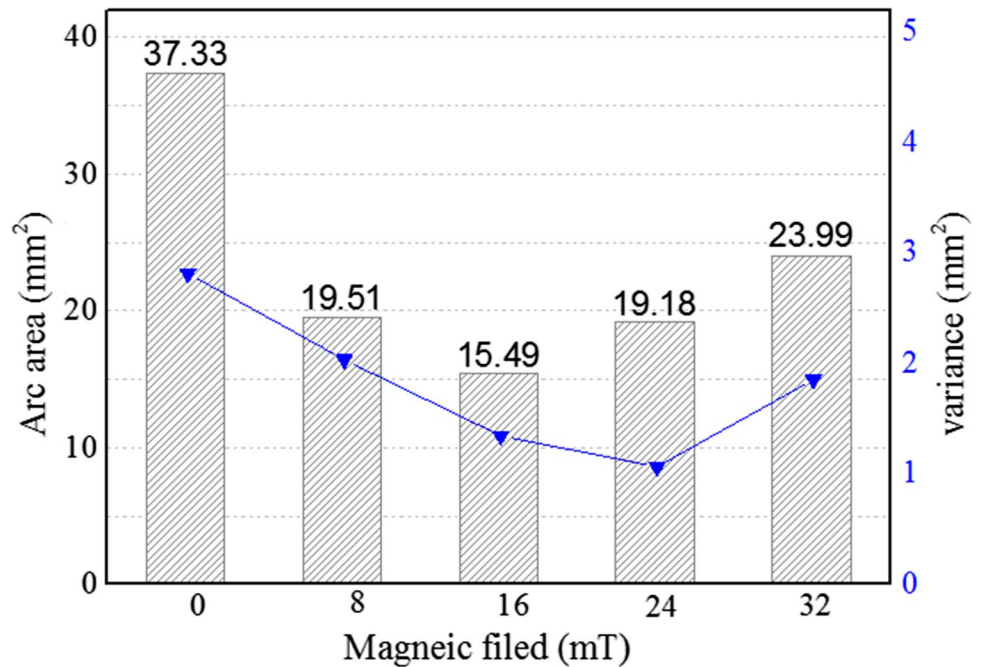


Fig. 8 The droplet transfer process in Laser-MIG welding

downward and backward. Herein, the droplet detachment size was 1.033 mm, similar to that of the wire. The droplet transfer form then changes from short-current transfer to meso-spray transfer, and the frequency of droplet transfer increases. Figure 9e shows the influence of 32-mT external magnetic fields on the droplet, where the droplet detachment diameter was 1.098 mm, and the frequency increased. However, during this process, the stability of the droplet

transfer worsened, and the droplet was divided into two parts, with one part moving upward along the welding wire. Furthermore, the detachment droplet shape was unstable producing an incomplete fusion welding defect.

As seen in Fig. 9, the droplet size was larger at 0 mT than between 8 and 24 mT, and unstable at 32 mT, indicating that the droplet spread unevenly on the weld beam at high welding speeds. The experiment can be divided into three cases:

Fig. 9 Effects of different magnetic fields on droplet transfer performance

Magnetic field	Droplet Performance				Average arc diameter (r)
(a) 0 mT					1.835 mm
(b) 8 mT					1.578 mm
(c) 16 mT					1.235 mm
(d) 24 mT					1.033 mm
(e) 32 mT					1.098 mm
Case 1	Insufficient Droplet transfer		Case 2		Appropriate Droplet transfer
Case 3	Excessive Droplet transfer				

insufficient droplet transfer, appropriate droplet transfer, and excessive droplet transfer. Although the welding quality was insufficient in cases 1 and 3 and excellent in case 2, the mechanisms in cases 1 and 3 were different, considering that the surface tension force was too large in case 1 to prevent the droplet from detaching from the wire, whereas the wire melting speed was too fast in case 3 to fit the droplet transfer process.

In conclusion, the trajectory of the droplet changes with an increase in the external magnetic field (case 2). A suitable external magnetic field (24 mT) can efficiently improve the droplet transfer frequency and decrease the droplet detachment size. Considering a small magnetic field (8 mT) cannot change the droplet transfer form, and an excessive external magnetic field (case 3) decreases the droplet transfer process stability; the most appropriate magnetic field parameter was 24 mT.

4.3.2 Influence of the magnetic field on the droplet transfer behavior

The main force acting on the droplet during the droplet transfer process can be identified based on the theoretical

background. However, considering the droplet behavior and the force changes as the external magnetic field increases, the direction, and magnitude of these forces should be clearly identified to study the relationship between the droplet behavior and the external magnetic field.

The direction of the forces depends on the location of the welding head. Figures 10a, b, and c show the forces acting on the droplet during MIG welding when the laser was added, and when an external magnetic field is added during hybrid welding, respectively. The direction of F_g is vertically downward, and its magnitude increases as the droplet size increases. F_g reaches its maximum value before droplet detachment and can be calculated using Eq. (3). The direction of F_v is vertically upward, which is consistent with the steam movement direction. According to Eq. (4), F_v is negligible when DLA is larger than the droplet diameter. The direction of F_{em} is determined by the arc characteristics and position of the droplet, which is parallel to the arc direction and can be calculated using Eq. (5). F_σ acts on the interfaces between solid, liquid, and gas, and its direction points to the contraction direction at the tangent of the three interfaces (liquid–gas, solid–liquid, and gas–solid). The direction of the

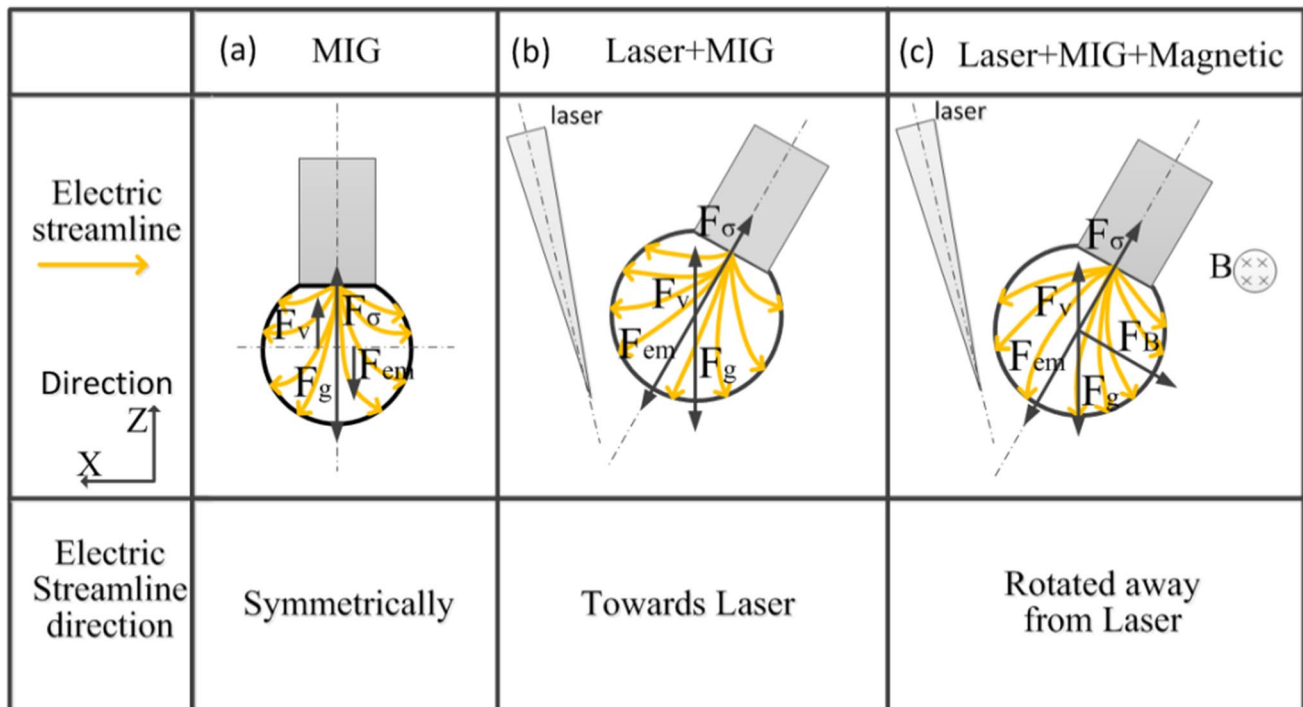


Fig. 10 Schematic of the forces acting on the pendant droplet in different welding processes

resultant force among the entire interface is from the center of the droplet to the welding wire, which can be calculated using Eq. (2). The external magnetic field is a transverse magnetic field. According to the left-hand rule, the direction of the F_B is perpendicular to the current direction, that is, backward and downward, and can be calculated using Eq. (6).

Based on the information from the HSC images seen in Fig. 11, the maximum droplet detachment size, angle of the arc-cover area, and detachment cycle are influenced by the external magnetic field, which was used to calculate the forces acting on the droplet under different magnetic fields. The values of the forces under different external magnetic fields are listed in Table 4.

The droplet detachment criterion is given by the following:

$$\vec{F}_D = \vec{F}_g + \vec{F}_{em} + \vec{F}_v + \vec{F}_B > \vec{F}_\sigma \quad (7)$$

The droplet transfer form is a short-circuit transfer if $F_D < F_\sigma$ before the droplet contacts the molten pool, wherein the surface tension $F_{\sigma m}$ between the droplet and the molten pool promotes droplet detachment. This force is determined by the contact area between the droplet and the molten pool, which is proportional to the contact time. Hence, the contact time between the droplet and the molten pool is proportional to the difference between F_D and F_σ .

The forces acting on the droplet without a magnetic field are shown in Fig. 11a. Considering F_σ is larger than

the resultant force of F_D , the droplet cannot be detached from the wire. Moreover, the contact time between the droplet and the molten pool was so long that the stability of the droplet transfer decreased. The external Lorentz force F_B is the detachment force, with a contrasting direction to that of F_σ , which can reduce the contact time between the droplet and the molten pool. The forces acting on the droplet at $B = 8$ mT are shown in Fig. 11b. F_B is smaller than F_σ and had no significant impact on the droplets, with a direction almost perpendicular to F_σ . As the magnetic field increases, F_B rapidly increases. The forces acting on the droplet when $B = 16$ mT were similar to those at 8 mT. F_B was over 50% smaller than F_σ . As seen in Fig. 11c, when $B = 24$ mT, F_σ was 28.2% larger than F_D , which promotes the best contact time between the droplet and the molten pool. The contact time was so small that the droplet transfer mode changes from short-circuit transfer to meso-spray transfer, thereby improving the droplet transfer stability. This phenomenon is mainly attributed to changes in the Lorentz force direction during droplet rotation, which increases the effective detachment energy. The forces acting on the droplet at $B = 32$ mT are shown in Fig. 11d. The direction of F_B was backward and upward. This process was not conducive to the separation of droplets from the wire. The droplet moves backward and is divided into two parts under an excessive magnetic field. The droplet moved upward along the wire, leading to the occurrence of the droplet department. Therefore,

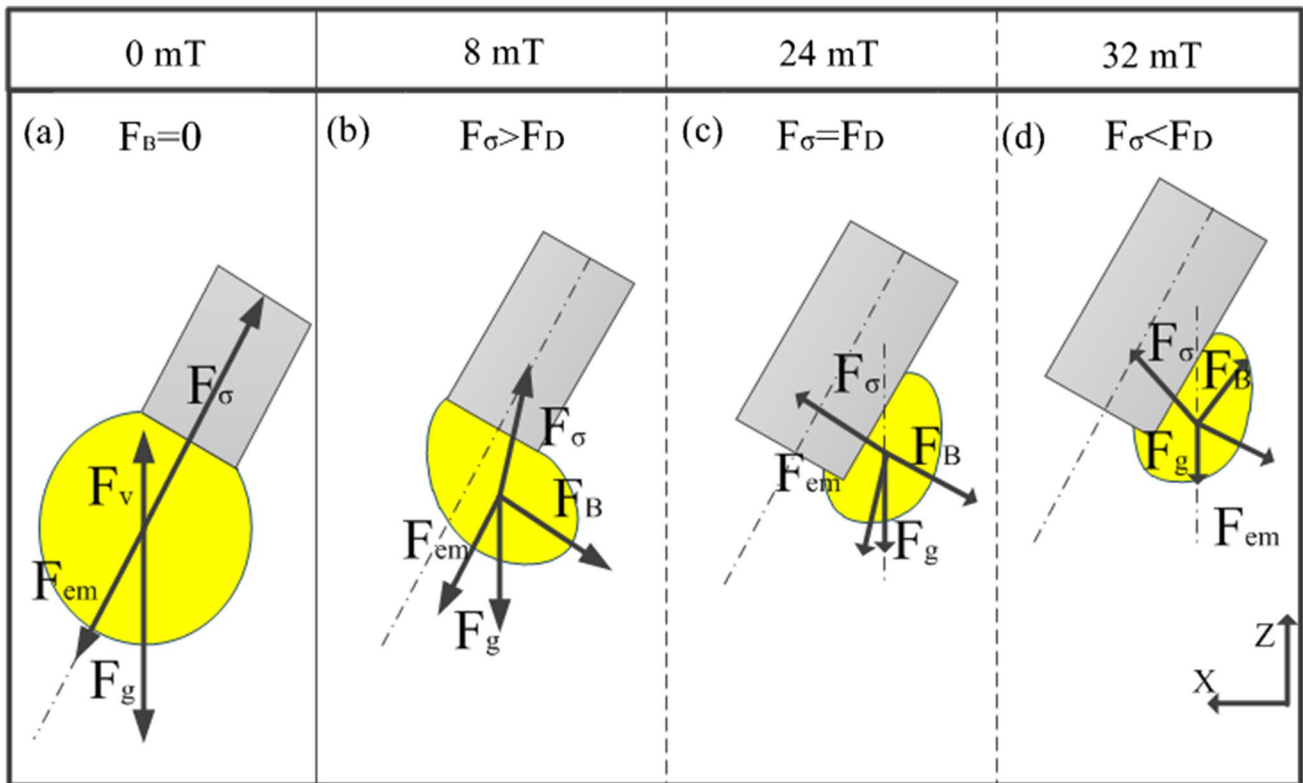


Fig. 11 Main forces acting on the droplet under different external magnetic fields. **a** Without magnetic field. **b** Insufficient magnetic field (8 mT). **c** Appropriate magnetic field (24 mT). **d** Excessive magnetic field (32 mT)

an external magnetic field of 24 mT can promote effective detachment energy improvement and droplet transfer stability.

Table 4 The forces on the droplet under different magnetic field

Magnetic field	$F_v(N)$	$F_g(N)$	$F_σ(N)$	$F_{em}(N)$	$F_B(N)$
0mT	0	1.42×10^{-4}	4.99×10^{-3}	1.93×10^{-3}	0
8mT	0	8.27×10^{-5}	4.99×10^{-3}	1.48×10^{-3}	1.55×10^{-3}
16mT	0	3.96×10^{-5}	4.99×10^{-3}	9.14×10^{-4}	2.48×10^{-3}
24mT	0	2.32×10^{-5}	4.99×10^{-3}	4.57×10^{-4}	3.11×10^{-3}
32mT	0	2.78×10^{-5}	4.99×10^{-3}	6.13×10^{-4}	4.41×10^{-3}

5 Conclusion

In this study, we investigated the effect of transverse magnetic fields of 0 mT, 8 mT, 16 mT, 24 mT, and 32 mT on the arc performance, droplet transfer, and weld bead

appearance during the laser-MIG hybrid welding of Ti-6Al-4 V. $B = 24$ mT was observed to be the most appropriate magnetic field parameter during the laser-MIG parameters (2 kW, 160 A, 2 m/min). The main results are summarized as follows:

- (1) An appropriate external magnetic field (case 2) can improve the weld quality and reduce welding defects, such as incomplete fusion and undercutting. However, an excessive external magnetic field (case 3) causes new welding defects, such as spatter, hump, and incomplete fusion.
- (2) The arc performance depends on the distribution of the electric streamlines. An appropriate transverse magnetic field (24 mT) can shrink the arc and improve its stability, causing the arc shape to change from a bell to a dish. The arc shrinkage and stability further affect the stability of the welding process and the wire melting speed.
- (3) The droplet transfer cycle transfer size decreased, which led to a reduction in the contact time between the droplet and molten pool. The droplet transfer form

changes from short-circuit transfer to meso-spray transfer, which implies that the droplet transfer stability increases at 24 mT.

- (4) The external magnetic field is mainly attributed to changes in the Lorentz force direction during droplet rotation, which increases the effective detachment energy and decreases the contact time between the droplet and molten pool, and promotes an effective detachment energy improvement and droplet transfer stability.

Acknowledgements The authors would also like to thank the anonymous referees for their valuable comments.

Funding This research has been supported by National Natural Science Foundation of China (NSFC) under Grant Nos. 51861165202 and 51721092.

Declarations

Ethics approval and consent to participate. Not applicable.

Conflict of interest The authors declare no competing interests.

References

- Gurrappa I (2003) Characterization of titanium alloy Ti-6Al-4V for chemical, marine and industrial applications. *Mater Charact* 51:131–139. <https://doi.org/10.1016/j.matchar.2003.10.006>
- Traverso P, Canepa E (2014) A review of studies on corrosion of metals and alloys in deep-sea environment. *Ocean Eng* 87:10–15. <https://doi.org/10.1016/j.oceaneng.2014.05.003>
- Gao Z, Jiang P, Wang C, Shao X, Pang S, Zhou Q, Li X, Wang Y (2016) Study on droplet transfer and weld quality in laser-MIG hybrid welding of 316L stainless steel. *The International Journal of Advanced Manufacturing Technology* 88:483–493. <https://doi.org/10.1007/s00170-016-8774-2>
- B. Chang, Z. Yuan, H. Pu, H. Li, H. Cheng, D. Du, J. Shan (2017) “A comparative study on the laser welding of Ti6Al4V alloy sheets in flat and horizontal positions.” *Applied Sciences* 7: <https://doi.org/10.3390/app7040376>.
- Caiazza F, Cardaropoli F, Alfieri V, Sergi V, Argenio P, Barbieri G (2017) Disk-laser welding of Ti-6Al-4V titanium alloy plates in T-joint configuration. *Procedia Engineering* 183:219–226. <https://doi.org/10.1016/j.proeng.2017.04.024>
- X. Su, W. Tao, Y. Chen, and J. Fu (2018) “Microstructure and tensile property of the joint of laser-MIG hybrid welded thick-section TC4 alloy.” *Metals* 8: <https://doi.org/10.3390/met8121002>.
- Sun Y, Luo G, Zhang J, Wu C, Li J, Shen Q, Zhang L (2018) Phase transition, microstructure and mechanical properties of TC4 titanium alloy prepared by plasma activated sintering. *J Alloy Compd* 741:918–926. <https://doi.org/10.1016/j.jallcom.2018.01.197>
- Liwei W, Yingchao S, Zhimin L, Dianlong W, Jun X, Dejun Y (2019) Numerical simulation and experiments on the behavior and mechanism of laser-assisted droplet transfer. *Opt Lasers Eng* 122:303–311. <https://doi.org/10.1016/j.optlaseng.2019.06.019>
- Liu S, Zhang F, Dong S, Zhang H, Liu F (2018) Characteristics analysis of droplet transfer in laser-MAG hybrid welding process. *Int J Heat Mass Transf* 121:805–811. <https://doi.org/10.1016/j.ijheatmasstransfer.2018.01.047>
- Liu LM, Yuan ST, Li CB (2013) Effect of relative location of laser beam and TIG arc in different hybrid welding modes. *Sci Technol Weld Joining* 17:441–446. <https://doi.org/10.1179/1362171812y.0000000033>
- Zhang W, Hua X, Liao W, Li F, Wang M (2014) Behavior of the plasma characteristic and droplet transfer in CO2 laser–GMAW–P hybrid welding. *The International Journal of Advanced Manufacturing Technology* 72:935–942. <https://doi.org/10.1007/s00170-014-5731-9>
- Wang J, Wang C, Meng X, Hu X, Yu Y, Yu S (2011) Interaction between laser-induced plasma/vapor and arc plasma during fiber laser-MIG hybrid welding. *J Mech Sci Technol* 25:1529–1533. <https://doi.org/10.1007/s12206-011-0410-3>
- Chen YB, Feng JC, Li LQ, Li Y, Chang S (2013) Effects of welding positions on droplet transfer in CO2 laser–MAG hybrid welding. *The International Journal of Advanced Manufacturing Technology* 68:1351–1359. <https://doi.org/10.1007/s00170-013-4926-9>
- G. Tang, H. Chen, X. Yang, and L. Shen (2018) “Effects of different welding process on the electronic temperature of plasma and weld shape during laser-MIG hybrid welding of A7N01P-T4 aluminum alloy.” *Journal of Laser Applications* 30: <https://doi.org/10.2351/1.5004434>.
- Chen J, Chen Q, Wu C (2020) Study of high-speed pulsed gas metal arc welding assisted by external magnetic-field. *Sci Technol Weld Joining* 25:564–570. <https://doi.org/10.1080/13621718.2020.1774994>
- Z. Zhengwu, M. Xiuquan, W. Chunming, and M. Gaoyang (2020) “Grain refinement and orientation alternation of 10 mm 316L welds prepared by magnetic field assisted narrow gap laser-MIG hybrid welding.” *Materials Characterization* 164: <https://doi.org/10.1016/j.matchar.2020.110311>.
- Chen R, Wang C, Jiang P, Shao X, Zhao Z, Gao Z, Yue C (2016) Effect of axial magnetic field in the laser beam welding of stainless steel to aluminum alloy. *Mater Des* 109:146–152. <https://doi.org/10.1016/j.matdes.2016.07.064>
- V. Avilov, A. Fritzsche, M. Bachmann, A. Gumenyuk, and M. Rethmeier (2016) “Full penetration laser beam welding of thick duplex steel plates with electromagnetic weld pool support.” *Journal of Laser Applications* 28: <https://doi.org/10.2351/1.4944103>
- Z. Q. Guan, H. X. Zhang, X. G. Liu, A. Babkin, and Y. L. Chang (2019) “Effect of magnetic field frequency on the shape of GMAW welding arc and weld microstructure properties.” *Materials Research Express* 6: <https://doi.org/10.1088/2053-1591/ab2572>
- Chang YL, Liu XL, Lu L, Babkin AS, Lee BY, Gao F (2013) Impacts of external longitudinal magnetic field on arc plasma and droplet during short-circuit GMAW. *The International Journal of Advanced Manufacturing Technology* 70:1543–1553. <https://doi.org/10.1007/s00170-013-5403-1>
- Sun Q, Wang J, Cai C, Li Q, Feng J (2015) Optimization of magnetic arc oscillation system by using double magnetic pole to TIG narrow gap welding. *The International Journal of Advanced Manufacturing Technology* 86:761–767. <https://doi.org/10.1007/s00170-015-8214-8>
- Wang J, Sun Q, Feng J, Wang S, Zhao H (2016) Characteristics of welding and arc pressure in TIG narrow gap welding using novel magnetic arc oscillation. *The International Journal of Advanced Manufacturing Technology* 90:413–420. <https://doi.org/10.1007/s00170-016-9407-5>

23. Zhang X, Zhao Z, Mi G, Wang C, Li R, Hu X (2017) Effect of external longitudinal magnetic field on arc plasma characteristics and droplet transfer during laser-MIG hybrid welding. *The International Journal of Advanced Manufacturing Technology* 92:2185–2195. <https://doi.org/10.1007/s00170-017-0293-2>
24. Zhu, X. Ma, C. Wang, and G. Mi, “Modification of droplet morphology and arc oscillation by magnetic field in laser-MIG hybrid

welding,”(2020) *Optics and Lasers in Engineering* 131: <https://doi.org/10.1016/j.optlaseng.2020.106138>.

Publisher's note Springer Nature remains neutral with regard to jurisdictional claims in published maps and institutional affiliations.